
Research Article: New Research | Sensory and Motor Systems

Arginine Vasopressin-Containing Neurons of the Suprachiasmatic Nucleus Project to CSF

<https://doi.org/10.1523/ENEURO.0363-20.2021>

Cite as: eNeuro 2021; 10.1523/ENEURO.0363-20.2021

Received: 19 August 2020

Revised: 30 December 2020

Accepted: 4 January 2021

This Early Release article has been peer-reviewed and accepted, but has not been through the composition and copyediting processes. The final version may differ slightly in style or formatting and will contain links to any extended data.

Alerts: Sign up at www.eneuro.org/alerts to receive customized email alerts when the fully formatted version of this article is published.

Copyright © 2021 Taub et al.

This is an open-access article distributed under the terms of the Creative Commons Attribution 4.0 International license, which permits unrestricted use, distribution and reproduction in any medium provided that the original work is properly attributed.

1 **Title:**

2

3 **Arginine Vasopressin-Containing Neurons of the Suprachiasmatic Nucleus**
4 **Project to CSF**

5

6 **Abbreviated title: SCN vasopressin neurons project to CSF**

7

8 **Authors:**

9

10 **Alana Taub¹, Yvette Carbajal², Kania Rimu², Rebecca Holt²,**
11 **Yifan Yao¹, Amanda L. Hernandez¹, Joseph LeSauter² and Rae Silver^{1,3}**

12

13 ¹Departments of Psychology, Columbia University, New York, NY, 10027

14 ²Department of Neuroscience, Barnard College, New York, NY 10027.

15 ³Department of Pathology and Cell Biology, Graduate Faculty, Columbia University
16 Medical School, New York, NY 10032.

17

18 **Corresponding Author:**

19 Rae Silver, Department of Psychology, Mail Code 5501, Columbia University, 1190
20 Amsterdam Avenue, New York, NY 10027, eMail: Rae.Silver@columbia.edu.

21

22 Number of figures: 11 (10 for main manuscript + visual abstract)

23 Number of tables: 1

24 Number of words

25 Abstract 242

26 Introduction 635

27 Discussion 1070

28

29 **Acknowledgments:** Imaging was performed with support from the the Barnard College
30 Imaging Facility and the National Science Foundation (NSF 1828264).

31

32 **Conflicts of Interest:** The authors declare no competing financial interests.

33

34 **Funding sources:** This work was supported by National Science Foundation Grants
35 1256105 and 1749500 (to R.S.).

36

37

38

39

40

41

42

43 **Arginine Vasopressin-Containing Neurons of the Suprachiasmatic Nucleus**44 **Project to CSF**

45

46 **Visual abstract**47 Insert Visual Abstract Figure about here

48

49 While it is well established that there are robust circadian rhythms of arginine
50 vasopressin (AVP) in the cerebrospinal fluid (CSF), the route whereby the peptide
51 reaches the CSF is not clear. **(A)** AVP neurons constitute the largest fraction of the SCN
52 neuronal population. Here we show that processes of AVP-expressing SCN
53 neurons cross the epithelium of the 3rd ventricular wall to reach the CSF (black
54 arrows). Additionally, we report rostro-caudal differences in AVP neuron size and
55 demonstrate that the localization of cells expressing the clock protein PER2 extend
56 beyond the AVP population, thereby indicating that the size of this nucleus is somewhat
57 larger than previously understood. **(B)** Following lateral ventricle
58 (LV) injection of cholera toxin beta subunit (CT β , magenta) the retrograde tracer is seen
59 in AVP neurons of the SCN, supporting the anatomical evidence that AVP neuronal
60 processes directly contact the CSF.

61

62 **Abstract**

63 Arginine vasopressin (AVP) expressing neurons form the major population in the brain's
64 circadian clock located in the hypothalamic suprachiasmatic nucleus (SCN). They
65 participate in inter-neuronal coupling and provide an output signal for synchronizing

66 daily rhythms. AVP is present at high concentrations in the CSF and fluctuates on a
67 circadian timescale. While it is assumed that rhythms in CSF AVP are of SCN origin, a
68 route of communication between these compartments has not been delineated. Using
69 immunochemistry and cell filling techniques, we determine the morphology and location
70 of AVP neurons in mouse and delineate their axonal and dendritic processes. Cholera
71 toxin β subunit (CT β) tracer injected into the lateral ventricle tests whether AVP neurons
72 communicate with CSF. Most importantly, the results indicate that AVP neurons lie in
73 close proximity to the 3rd ventricle, and their processes cross the ventricular wall into the
74 CSF. We also report that contrary to widely held assumptions, AVP neurons do not fully
75 delineate the SCN borders as PER2 expression extends beyond the AVP region. AVP
76 neurons form a rostral prong originating in the SCN medial- and ventral-most aspect.
77 AVP is lacking in the mid-dorsal shell but does occur at the base of the SCN just above
78 the optic tract. Finally, neurons of the rostral SCN are smaller than those lying caudally.
79 These findings extend our understanding of AVP signaling potential, demonstrate the
80 heterogeneity of AVP neurons, and highlight limits in using this peptide to delineate the
81 mouse SCN.

82

83 **Significance Statement**

84 There is a high amplitude circadian rhythm of arginine vasopressin (AVP) in the
85 cerebroventricular fluid (CSF), presumed to be of suprachiasmatic nucleus (SCN) origin.
86 There is however, no known route of communication between these compartments. We
87 demonstrate that in the mouse SCN, processes of AVP neurons course toward the 3rd

88 ventricle and cross the ventricular wall to reach the CSF, thereby enabling
89 vasopressinergic signals to reach many brain regions bearing receptors for this peptide.
90 Also, the SCN extends beyond the borders delineated by AVP neurons and rostral AVP
91 neurons are smaller than caudal populations. The work extends our understanding of
92 AVP signaling potential, the heterogeneity of AVP neurons, and highlights limits in using
93 this peptide to delineate the SCN.

94

95 **Introduction**

96 The suprachiasmatic nucleus (SCN) of the hypothalamus, comprised of ~ 20,000
97 neurons, functions as a circadian clock, coordinating and synchronizing daily rhythms in
98 numerous bodily functions including metabolism, physiology, behavior, and hormone
99 secretion. These neurons contain a substantial array of peptides (Antle & Silver, 2005),
100 among which the best studied synthesize arginine vasopressin (AVP) (van den Pol &
101 Tsujimoto, 1985; Kalsbeek *et al.*, 2010). AVP-expressing neurons form the major
102 population of neurons in the SCN, and are estimated to constitute 37% of the nucleus
103 (Moore, 2013). Through most of its rostrocaudal extent, AVP perikarya lie within the
104 shell region (Moore, 2013; Lokshin *et al.*, 2015; Varadarajan *et al.*, 2018). It is widely
105 accepted that AVP neurons delineate the boundaries of the SCN and it is thought that
106 AVP neurons provide the major output signal from the SCN (Cassone *et al.*, 1988;
107 Daikoku *et al.*, 1992; Dai *et al.*, 1997; Abrahamson & Moore, 2001; Ramanathan *et al.*,
108 2006; Moore, 2013).

109 **Efferent connections of the SCN**

110 SCN efferents have been extensively studied (Moore, 2013; Morin, 2013) and more
111 specifically, the efferents of AVP neurons have also been explored (LeSauter & Silver,
112 1998; Kalsbeek *et al.*, 2010) The medial preoptic area, the periventricular and sub-
113 paraventricular nucleus, dorsomedial hypothalamus and paraventricular nucleus of the
114 thalamus have been identified as targets of SCN AVP neurons. Output from the SCN
115 influences visceral function (Ueyama *et al.*, 1999), REM sleep (Lee *et al.*, 2009), and
116 timing of the LH surge (Williams *et al.*, 2011). However, the extent to which all of these
117 connections originate from SCN or AVP neurons of other origins is not known.

118 **AVP expression in the SCN and CSF is rhythmic**

119 The transcriptional machinery of the core clockwork directly regulates rhythmic
120 expression of AVP in the SCN shell, but not in other AVP-producing neurons (Jin *et al.*,
121 1999; Silver *et al.*, 1999). The concentration of AVP in the cerebrospinal fluid (CSF),
122 thought to be of SCN origin, fluctuates daily with a peak in the morning (Schwartz &
123 Reppert, 1985; Söderstein *et al.*, 1985 ; Jolkkonen *et al.*, 1988; Stark & Daniel, 1989;
124 Kalsbeek *et al.*, 2010). Samples from rat CSF and blood definitively demonstrated
125 circadian rhythms in AVP levels in the cerebrospinal fluid (CSF) but not in the blood
126 (Schwartz *et al.*, 1983). This work established the importance of the SCN in producing
127 circadian rhythms in CSF AVP as SCN lesions abolished rhythmicity and reduced
128 measurable levels of the peptide but left open the possibility that neurons of the SCN
129 may trigger AVP release from some other neural sites. Also unknown was the route
130 whereby AVP of SCN origin might reach the CSF, a question in the present study.

131 **The present study**

132 While rhythmicity in CSF AVP levels is well established, the question of how AVP of
133 SCN origin might reach the CSF led to the present study. Much of the work on the SCN
134 has been done in coronal sections and this focus neglects the rostral and caudal-most
135 aspects of the nucleus, both of which are rich in AVP containing neurons (Riddle *et al.*,
136 2017; Varadarajan *et al.*, 2018). Additionally, in coronal sections it is difficult to visualize
137 the close and extended contact of the SCN with the wall of the 3rd ventricle. Here, we
138 first sought to better understand the full extent of AVP neurons in the mouse SCN. This
139 work pointed to dense AVP fibers projecting toward the CSF, a previously unidentified
140 target. To better characterize their axonal and dendritic processes, we filled AVP
141 neurons with biocytin and characterized their afferent and efferent processes using
142 confocal microscopy. To assess communication of AVP neurons with CSF,
143 immunocytochemistry was used to label the ventricular wall and the tracer cholera toxin
144 beta subunit (CT β), was injected into the lateral ventricle and SCN AVP cells bearing
145 the tracer were identified.

146

147 **Methods and Materials**

148 **Animals and Housing**

149 Two strains of mice were used to optimize detection of markers of interest with our
150 multi-label protocols. For detection of PER2, we used adult C57BL/NJ mice (Jackson
151 Laboratory, Bar Harbor, ME); for cell filling with biocytin, laboratory bred 15 day old
152 *Per1*-GFP mice (Kuhlman *et al.*, 2000) were used. Mice were group-housed (4/cage) in
153 translucent propylene cages (48 x 27 x 20 cm) in a colony room with a 12:12 hr
154 light:dark cycle at 21 \pm 2 °C and provided with free access to food and water. All

155 procedures were approved by the Columbia University Animal Care and Use
156 Committee.

157

158 **Localization of AVP neurons and efferents**

159 Mice were anesthetized with 100 mg/kg of ketamine and 10 mg/kg of xylazine and
160 perfused transcardially with 50 ml of saline followed by 75 ml of 4% paraformaldehyde.
161 Brains were postfixed overnight at 4°C and then cryoprotected in 20% sucrose in 0.1 M
162 phosphate buffer .9% saline (PBS). For immunocytochemistry (ICC) sections (50 μ m) were
163 cut in the sagittal, horizontal or coronal planes on a cryostat (Microm HM 500M,
164 Walldorf, Germany) and collected into 0.1 M PBS. The brain sections were processed
165 as free-floating sections in 24 well plates. For single label ICC, sections were washed in
166 0.1M phosphate buffer 0.9% saline (PBS) +0.1 % Triton-X 100 and then blocked with
167 normal donkey serum for 1 hr on a shaker at room temperature. Sections were washed
168 3 x10 min in PBS and placed in a 0.3%(PBST) solution containing rabbit anti-AVP
169 antibody at 4°C for 48 hrs. Sections were washed (3x) and incubated for 2 hr at RT in
170 .3%PBST containing the appropriate secondary antibody. Sections were washed in PB,
171 mounted, dehydrated in ethanol solutions, cleared in CitriSolve (Fisher Scientific) and
172 coverslipped with Krystalon (EM Diagnostics, Gibbstown, NJ). For double label ICC, the
173 same procedure was used except primary antibodies were either mouse anti-AVP and
174 rabbit anti-PER2; mouse anti-AVP and rabbit anti-S100 β or rabbit anti-AVP and goat
175 anti-CT β . The appropriate fluorescent secondaries were used (Table 1).

176

177 **AVP in relation to the ependymal wall**

178 To assess AVP fibers in supra and sub-ependymal zones of the 3rd ventricle, we
179 observed AVP and S100 β labelled sections (n=5 female mice). S100 β stains ependymal
180 cells (Didier *et al.*, 1986; Carlen *et al.*, 2009; Lavado & Oliver, 2011).

181

182 **Biocytin filling of patched AVP cells to determine morphology of AVP neurons**

183 To determine the morphology of AVP neurons and their axonal and dendritic
184 projections, *Per1*-GFP mice were sacrificed by cervical dislocation between ZT 12 and
185 15 (when PER1-GFP expression is high), and cells were patched and filled with biocytin
186 as described for GRP-GFP cells (Drouyer *et al.*, 2010). For immunocytochemistry of
187 sections bearing biocytin-filled cells tissue was incubated overnight at 4°C with Cy2
188 streptavidin (Jackson ImmunoResearch, West Grove, PA) in PBST, then processed as
189 above except primary antibodies were guinea pig anti-AVP and rabbit anti-GFP, stained
190 with the appropriate secondary antibodies.

191

192 **Analysis of Biocytin filling**

193 Each filled cell was examined throughout the z stack using confocal microscopy to
194 assess whether it was single, double or triple labeled for biocytin (green), PER1-GFP
195 (magenta) and AVP (blue). Of 73 cells filled with biocytin in 9 animals, 53 were PER1-
196 GFP positive and 20 were PER1-GFP negative. Of the 53 PER 1-GFP positive cells, 30
197 were AVP+ and 23 were AVP-. The 20 PER1-GFP negative cells were also AVP
198 negative. Axons originate from the soma or from a proximal dendrite and are very fine
199 and beady. Dendrites are larger and possess spines, swellings and/or appendages
200 [described in (van den Pol, 1980)].

201

202 **Measuring cell size**

203 In the initial study, confocal microscopy was used to measure the perimeter of distinct
204 populations of AVP neurons, enabling comparison with previous studies of this
205 population (Campos *et al.*, 2014, Moore *et al.*, 2002). Images were taken from the
206 rostral- and caudal-most aspects, at the largest extent of the SCN - the mid-region in
207 sagittal sections (2 sections/SCN, n=8 SCNs). The cells were measured at their
208 greatest extent, where a distinct nucleus was seen on the 1 μ m z-axis optical section.
209 The perimeter was determined using the “Annotations and Measurements” tool on NIS-
210 Elements Advance Research software. Seven to 21 cells were measured/region for
211 each brain section (total N= 76 rostral, 89 caudal cells). For volumetric measures, a new
212 set of confocal images of AVP stained SCNs were imported into the imaging software
213 Aivia (Version 9, DRVISION Technologies LLC, Bellevue, WA). The segmentation
214 output in the pixel classifier tool allows for visualization of the cells in 3D and was used
215 to measure volume of individual rostral (N=88) and caudal (N=101) cells.

216

217 **CT β tracer, lateral ventricle injection site**

218 While CT β is an anterograde and retrograde tracer, it behaves primarily as a retrograde
219 tracer at the doses and sites described here (see (Leak & Moore, 2012) for extended
220 discussion and explanation). CalB-GFP mice were anesthetized with 100 mg/kg of
221 ketamine and 10 mg/kg of xylazine at ZT14 and prepared for aseptic surgery. The head
222 was shaved and the mouse was positioned in a stereotaxic apparatus (David Kopf
223 Instruments, Tujunga, CA). Injections were aimed at the lateral ventricle (AP +1.1, ML

224 +0.7 from Bregma, DV -3.0 from the top of the skull). Pressure injections of 4 μ l of CT β
225 (1% low salt solution, List Biologicals, Campbell, CA) were made with a 10 μ l syringe
226 (Hamilton Co., Reno, NV) at a rate of 2 μ l per min. The cannula was left in the brain at
227 the end of the infusion for an additional 2 min and removed slowly over 1 min to
228 minimize tracer diffusion upon needle withdrawal. The animals were sacrificed 7 days
229 following surgery. Mice (n=8) were injected with CT β . The injection penetrated the
230 lateral septum in 3 brains but was strictly localized to the lateral ventricle in 5 injections
231 (Fig. 1).

232

233 Insert Figure 1 about here

234

235 **Microscopy**

236 Immunofluorescent labeling was examined on a Nikon Eclipse E800 (Morrell
237 Instruments, Melville, NY) microscope using the filters 480 \pm 40 nm for Cy2, 560 \pm 40 nm
238 for Cy3 and 620 \pm 40 nm for Cy5. Images were captured with a USB-3 DMK33UX174
239 camera (Morrell Instruments) using the Nikon NIS-Elements Basic Research software.
240 To identify AVP dendrites and axons in biocytin-filled cells, and to determine their
241 relation to the CSF, images were taken on a Nikon Eclipse Ti2E confocal microscope
242 (Nikon, Melville, NY) equipped with a LUNV Laser unit and an argon-krypton laser using
243 the excitation wavelengths 488 nm for Cy2, 561 nm for Cy3 and 638 nm for Cy5. NIS
244 Elements Advanced Research software was used to visualize the z-stacks. Confocal
245 images of sections from CT β -injected mice were analyzed to determine the
246 colocalization of CT β with AVP. The images were imported into Photoshop (Adobe

247 Photoshop CS. Berkeley, CA). Single labelled CT β and AVP and double labelled cells
 248 were counted by two experimenters (agreement: $93 \pm 2\%$).

249

250 **Image analysis**

251 For visualization of cells and/or fibers, we used Photoshop. To recover lost details in
 252 dark and bright areas of the image “Shadows” and “Highlights” were adjusted in the
 253 “Image-Adjustment-Levels” dialog box in Photoshop, by dragging the black and
 254 white “Input Levels” to the edge of the first group of pixels on either end of the
 255 histogram (Figs. 4 and 5). The function of “Shadows” and “Highlights” is to brighten
 256 areas of shadow and darken areas of brightness based on surrounding pixels; it does
 257 not simply lighten or darken an image (Adobe Photoshop CS6). For color images,
 258 “Shadows” and “Highlights” were manipulated for each color separately. Grayscale
 259 images were inverted prior to these visual optimizations.

260

261 Table 1. Primary and secondary antibodies used. *catalog number as RRID not
 262 available.

Antibodies	Host	Dilution	Company	RRID
AVP	Mouse	1:500	Santa Cruz Biotechnology, Santa Cruz, CA	sc-390723 *
AVP	Rabbit	1:5000	Immunostar, Hudson, WI	AB_572219
AVP	Guinea Pig	1:5000	Peninsula Laboratories, San Carlos, CA	AB_2313978
PER2	Rabbit	1:500	EMD Millipore, Temecula, CA	AB_1587380
S100 β	Rabbit	1:1	Dako, Carpinteria, CA	AB_1587380
CT β	Goat	1:500	Lists Biologicals, Campbell, CA	AB_10013220
Cy2	Rabbit	1:200	Jackson <u>Immunoresearch</u> , West Grove, PA	AB_2340612

Cy3	Mouse	1:200	Jackson <u>Immunoresearch</u> , West Grove, PA	<u>AB_2340813</u>
Cy3	Rabbit	1:200	Jackson <u>Immunoresearch</u> , West Grove, PA	AB_2307443
Cy3	Goat	1:200	Jackson <u>Immunoresearch</u> , West Grove, PA	AB_2307351
CY5	Guinea Pig	1:200	Jackson <u>Immunoresearch</u> , West Grove, PA	AB_2340462
Other Products				
Normal donkey serum		1:100	Jackson <u>Immunoresearch</u> , West Grove, PA	<u>AB_2337258</u>
NIS Elements software			Morrell Instruments, Melville, NY	SCR_002776
Photoshop			Adobe Photoshop CS. Berkeley, CA	SCR_014199

263

264 **Statistical analyses:**

265 Data for neuronal perimeter and volume of AVP neurons were measured using both
266 statistical inference and estimation statistics. For statistical inference, we used Student's
267 t-test for normally distributed data with equal variance, Welch's t-test for normally
268 distributed data with unequal variance and Mann-Whitney U test for data lacking normal
269 distribution. For these analyses, outliers were removed (for perimeter, 6 rostral and 4
270 caudal; for volume, 7 rostral and 2 caudal) using the Tukey method [quartile 1 and 3 \pm
271 (1.5*interquartile range)]. For both perimeter and volume distribution normality was
272 analyzed by the Kolmogorov-Smirnov Test and equality of variances was calculated by
273 F test. For perimeter measures, data for both rostral and caudal are normally distributed
274 ($D_{\text{rostral}}=0.94$, $P=0.53$; $D_{\text{caudal}}=0.09$, $p=0.46$) but have unequal variance ($S_{\text{rostral}}=15.21$;

275 $S_{\text{caudal}}=35.22$, $F=0.43$, $p=0.004$). Data grouped within individual SCNs are normally
276 distributed ($D_{\text{rostral}}=0.22$, $P=0.75$; $D_{\text{caudal}}=0.13$, $p=0.99$) and have equal variance
277 ($S_{\text{rostral}}=7.8$; $S_{\text{caudal}}=5.9$, $F=1.31$, $p=0.73$). For volumetric measures, data for all neurons
278 are normally distributed for rostral cells ($D_{\text{rostral}}=0.09$, $P=0.49$), but not for caudal cells
279 ($D_{\text{caudal}}=0.14$, $p=0.02$). The volumetric measures within individual SCN are normally
280 distributed ($D_{\text{rostral}}=0.17$, $P=0.98$; $D_{\text{caudal}}=0.22$, $p=0.86$) and have equal variance
281 ($S_{\text{rostral}}=3432.68$; $S_{\text{caudal}}=11576.27$, $F=0.3$, $p=0.21$]. Estimation statistics were run using
282 <https://www.estimationstats.com/>. Mean difference was selected for effect size and
283 5000 bootstrap samples were run using bias-corrected and accelerated confidence
284 interval (CI) protocols [95% CI lower, upper range] (Ho *et al*, 2019).

285

286 **Results**

287 **AVP in SCN**

288 Because AVP-containing neurons are often used to delineate the extent of the SCN, we
289 investigated the accuracy of this protocol by comparing the area of PER2 expression at
290 its peak (ZT12-14) to that of AVP-ir. In sagittal sections, we were surprised to find that
291 at mid and lateral levels of the nucleus, the area of PER2 expression extends well
292 beyond that delineated by AVP (Fig. 2). Most medially PER2 expression corresponds to
293 the area delineated by AVP neurons (not shown).

294

295 [Insert Figure 2 about here](#)

296

297 As previous studies suggest a relationship between the size of SCN neurons and their
298 location within the nucleus (Campos *et al.*, 2014), we also examined the size of AVP
299 neurons in the rostral versus the caudal SCN measuring both perimeter and volume.
300 The results indicate that neurons lying caudally are larger than rostral ones for both
301 measures and this held true whether statistical inference or estimation statistics were
302 applied (Fig. 3).

303

304 Insert Figure 3 about here

305

306 Measures for perimeter are shown in Fig.(3B). The statistical results are as follows: for
307 cell perimeter (FIG 3B, upper panel), Welch's $t_{(69,84)} = 5.48$, $p = 1.7e-7$ [with outliers
308 included, the difference is also significant (Welch's $t_{(75,88)} = 3.53$, $p = 0.0005$)]. CI
309 unpaired mean difference is 4.36 [95.0%CI 2.84, 5.91, $p < 0.00001$]. For mean cell
310 perimeter within individual SCNs (FIG 3B, lower panel) Student's paired $t_{(7)} = 5.76$,
311 $*p = 0.0007$. Paired mean difference between rostral and caudal is 3.7 [95.0%CI 2.62,
312 4.94], $p < 0.00001$. For volume per cell (Fig. 3BC, upper panel), $Z_{(81,89)} = 3.65$, $p = 0.0003$
313 [with outliers included, the difference is also significant ($Z_{(87,100)} = 2.73$, $p = 0.006$)]. CI
314 unpaired mean difference = 1.26×10^2 [95.0%CI 72.5, 1.84×10^2], $p < 0.00001$. For mean
315 volume within individual SCNs (Fig. 3C, lower panel), Student's paired $t_{(5)} = 3.44$,
316 $*p = 0.02$. Paired mean difference = 1.17×10^2 [95.0%CI 61.2, 1.8×10^2], $p = 0.03$.

317

318 The precise localization of AVP neurons in the main body of the SCN is shown in 7
319 serial sagittal sections (50 μ m) through the extent of the SCN from the medial-most to

320 the lateral-most aspect, in two animals sectioned at slightly different angles.

321 Additionally, a substantial rostral prong is shown in both sagittal and horizontal views

322 (Fig. 4).

323

324 Insert Figure 4 about here

325

326 While the SCN is embedded within the hypothalamus for most of its extent, most

327 medially, it is separated from the rest of the hypothalamus by the 3rd ventricle (Fig. 4,

328 animal #1 and #2, images 1,2). At its dorsal aspect the SCN abuts the 3rd ventricle,

329 most evident when the section is cut perfectly parallel to the midline (Fig. 4, animal #1,

330 images 1 and 2). In animal 1, in sections cut parallel to the midline, the medial SCN is

331 located right below the 3rd ventricle (images 1 and 2). At the mid-level (images 3 to 5),

332 the rostral pole of the SCN abuts the 3rd ventricle and the main body is caudal to the

333 ventricle. Laterally (image 7), the SCN lies entirely within the hypothalamic parenchyma

334 and is no longer in contact with the 3rd ventricle. In animal 2, in sections cut at a

335 different angle, the 3rd ventricle is seen medially (images 1-3), but no longer visible at

336 images 4-7.

337 At the medial aspect of the SCN, AVP neurons occur throughout the SCN (Fig. 4A,

338 animal #1, image 1; animal #2, images 1 and 2) and these extend in a rostral prong that

339 originates in the ventral part of the nucleus and lies below the 3rd ventricle, just above

340 the optic chiasm (sagittal view Fig. 4A, animal #1, image 1, animal #2, images 1 and 2

341 and horizontal views Fig. 4B, animals #3 and 4 {black arrows}). The rostral prong

342 extends ~250 um rostrocaudally, 20-30µm dorsoventrally and ~80 µm mediolaterally. At

343 the mid-SCN at its greatest extent in the sagittal view, AVP neurons lie rostrally and
344 caudally, but are sparse in the core and in the mid-dorsal aspect (both animals, images
345 5; animal #2, image 6 {white arrows}). In addition, AVP neurons are present along the
346 base of the SCN (Fig. 4, both animals, images 4; animal #2, image 5 {arrow heads}). At
347 the lateral aspect, the AVP neurons are densely packed (both animals, image 7).

348

349 **Relation of AVP fibers to ependymal wall and CSF in coronal and sagittal**
350 **sections.**

351 In coronal sections, at its greatest extent, the SCN is rich in AVP neurons (Fig. 5A), and
352 many dendrites and axons course toward the CSF (Fig. 5B). In sagittal sections,
353 projections of AVP neurons travel rostrally toward the 3rd ventricle (Fig. 5C, arrow).
354 Close to the midline, the SCN lies directly above the optic chiasm and its dorsal aspect
355 abuts the 3rd ventricle (Fig. 5D). Here AVP fibers, appear to cross the ependymal wall
356 to reach the CSF in the 3rd ventricle.

357

358 Insert Figure 5 about here

359

360 **Morphology of axons and dendrites of AVP neurons**

361 To identify the axons and dendrites of AVP neurons, we patched and filled SCN
362 neurons with biocytin. Of the 30 AVP+ neurons studied, 22 had distinguishable axons
363 and dendrites. As previously described (van den Pol, 1980; Abrahamson & Moore,
364 2001), axonal processes of SCN origin are very thin and exhibit bulbous, irregularly

365 spaced varicosities along their entire length (Fig. 6). Dendrites are larger and possess
366 spines, swellings and/or appendages.

367

368 Insert Figure 6 about here

369

370 **SCN dendrites and/or axons crossing the ependymal wall**

371 To determine the terminal regions of SCN AVP neurons, we labelled sagittal sections
372 for AVP and S100 β , an ependymal wall marker. Some processes appear to terminate
373 subependymally while others cross into the 3rd ventricle. Both AVP axons (Fig. 7) and
374 dendrites (Fig. 8) extend through the ventricular wall both at the level of the SCN (Fig. 7
375 A, B, C and Fig. 8 A, C) or near the SCN (Fig. 7 D and 8 B, D). Terminal boutons can be
376 seen within the 3rd ventricle (Fig. 7 B' and C').

377

378 Insert Figures 7 and 8 about here

379

380 **CT β tracer in lateral ventricle labels SCN neurons**

381 As noted by (Leak & Moore, 2012), "The CSF contains neuroactive substances that
382 affect brain function and range in size from small molecule transmitters to peptides
383 and large proteins. CSF-contacting neurons are a well-known and universal feature
384 of non-mammalian vertebrates...". Given the evidence of AVP+ fibers directed to the
385 CSF, we next examined whether AVP cells would uptake the tracer CT β from the
386 ventricle. For this, we injected CT β into the lateral ventricle. Fig. 9 shows the cells that
387 took up the CT β tracer and colocalized with AVP (inset) in the mid SCN. The distribution

388 pattern of CT β in the SCN was similar in all 5 animals where injection was restricted to
389 the lateral ventricle.

390 Of the 4122 AVP and 2488 CT β cells evaluated, 15.3 ± 0.9 % AVP were co-labelled
391 with CT β . 25.5 ± 1.9 % CT β cells were co-labelled with AVP. The results point to
392 extensive input from CSF to SCN neurons bearing AVP.

393

394 [Insert Figure 9 about here](#)

395

396 **CT β in SCN Medial to Lateral**

397 Cells containing CT β are located mostly within the SCN shell where AVP cells are
398 present (Fig. 10). There are a few CT β cells in the very medial SCN (image 1). They are
399 located dorsally in the medial SCN (image 2). In the mid and lateral SCN, they are
400 located mostly within the dorsomedial region and are sparse in the SCN core (images 5-
401 7). They are also numerous in the dorsal area where AVP is sparser (image 5).

402

403 [Insert Figure 10 about here](#)

404

405 **Discussion**

406 **AVP fibers reach the CSF**

407 A major finding of the present study is that SCN AVP neurons course toward and even
408 terminate in the fluid space of the 3rd ventricle. This communication is most obvious in
409 sagittal sections through the SCN, especially near the brain midline. And while AVP
410 neurons have often been used to demarcate the outer borders of the SCN (Vandesande

411 *et al.*, 1975; Sofroniew & Weindl, 1980; Card & Moore, 1984; van den Pol & Tsujimoto,
412 1985), the sagittal view makes it clear that there are rhythmically expressing PER2
413 neurons that lie beyond this demarcation, especially at the lateral borders of the
414 nucleus.

415 Taken together the detailed description of AVP neurons in the SCN make 3 distinct
416 points: AVP cells are at the base of the core region of the SCN (Fig 4). Dorsomedial
417 region of the SCN shell is devoid of AVP neuron, AVP neurons extend rostrally along
418 the midline along a narrow protrusion that originates in the medial-most aspect of the
419 ventral SCN. While each of these details is modest, taken together they can correct
420 incomplete or erroneous anatomical information in previous less detailed work and can
421 provide the groundwork for fine-tuning future studies. Among the questions raised is the
422 nature and function of rhythmic SCN neurons that lie around the outer borders of the
423 SCN and whose existence was not previously realized.

424 As noted in the introduction, efferent projections of the SCN and more specifically,
425 efferents of AVP neurons of the SCN have been extensively studied (Berk & Finkelstein,
426 1981; Stephan *et al.*, 1981; Hoorneman & Buijs, 1982; Watts & Swanson, 1987; Watts
427 *et al.*, 1987; Kalsbeek *et al.*, 1993; Morin, 1994; Teclemariam-Mesbah *et al.*, 1999; Leak
428 & Moore, 2001; Moore and Silver, 1998). Although there are some differences among
429 species (Morin, 1994), AVP is a major component of the SCN in most species that have
430 been studied (Morin and Allen 2005). Furthermore, an important contribution of SCN to
431 rhythmic AVP levels in CSF has been known since the mid-1980's, though evidence of
432 the route of communication was lacking. To our knowledge however, there are no prior
433 reports of SCN processes reaching the CSF, though there is light and electron

434 microscopic evidence of (unidentified) somal processes inserted in the ependymal layer
435 or directly contacting the CSF space (Xiao *et al.*, 2005). This may be a consequence of
436 the difficulty of detecting the very fine SCN fibers that course in a rostro-caudal direction
437 (Figs. 4 and 5) especially when they lie right near the midline. The results are consistent
438 with evidence of volume transmission by the SCN and with prior studies. Specifically,
439 paracrine signaling with a role for AVP, has been demonstrated in culture preparations
440 of the SCN (Honma, 2020 [see Fig. 5], Maywood *et al.*, 2011, Tokuda *et al.*, 2018).
441 Furthermore, SCN grafts encapsulated in a polymer material can restore circadian
442 activity rhythms through volume transmission (Silver *et al.*, 1996). Finally, the SCN is
443 densely labeled with CSF injections of more than 20 nl of a tract tracer CT β (Leak &
444 Moore, 2012). More specifically, they showed that within 2 - 10 days of injection, the
445 CT β label appears in specific groups of neuronal perikarya in the telencephalon,
446 thalamus, hypothalamus and brainstem, many at a considerable distance from the
447 ventricles. They hypothesize that these observations support the view that ventricular
448 CSF is a significant channel for volume transmission and identify those brain regions
449 most likely to be involved in this process.

450

451 **AVP neurotransmitters**

452 The role of AVP in rhythmicity has been puzzling in view of the fact that AVP-deficient
453 Brattleboro rats display attenuated but normal circadian rhythms (Groblewski *et al.*,
454 1981; Brown & Nunez, 1989; Kalsbeek *et al.*, 2010). AVP-containing neurons express
455 GABA and prokineticin 2 (Masumoto *et al.*, 2006; Welsh *et al.*, 2010) pointing to the
456 possibility that these neurons play a broader role in the circadian timing system than

457 does the AVP protein itself. Mice in which the essential core clock gene *Bmal1* was
458 deleted in AVP neurons (Avp-Bmal1^{-/-} mice), had impaired circadian activity rhythms
459 (Mieda *et al.*, 2015) and a gradually expanded interval activity time upon being moved
460 from LD to DD. Bmal1 restoration in AVP neurons of the SCN using a recombinant
461 adeno-associated virus vector reversed the circadian impairment of Avp-Bmal1^{-/-} mice.
462 The results were interpreted to mean that the circadian oscillation persists at the cellular
463 level, but that mutual coupling among SCN neurons that regulate activity onset and
464 offset was impaired.

465

466 **Rhythms in SCN-regulated functions**

467 As noted by van den Pol (van den Pol, 2012) peptide release is difficult to study, as it is
468 seen independent of synaptic specializations, in dendrites, axonal boutons and axon
469 shafts. This is consistent with the possibility that axons and dendrites described here
470 (Fig. 7 and 8) both contribute to the rhythms of AVP in CSF. AVP has a role in the
471 regulation of hydration, blood pressure, body temperature, corticotropin release, and
472 has been implicated in depression, memory, social and sociosexual behavior and in sex
473 differences [reviewed in (de Vries & Miller, 1998; Kalsbeek *et al.*, 2010)]. The stress
474 system in the human brain has been implicated in depression and neurodegeneration
475 (Swaab *et al.*, 2005). The relationship of CSF levels of AVP to plasma levels is of
476 interest in studies of autism, suicide, (Brunner *et al.*, 2002) and personality disorders
477 (Coccaro *et al.*, 1998; Oztan *et al.*, 2018) and the two compartments seem to be
478 separately regulated (Kagerbauer *et al.*, 2013). Much remains to be investigated as
479 understanding the function of this compartment in the context of circadian rhythms
480 requires unravelling a sequence of steps involved in volume transmission. AVP is a

481 phylogenetically ancient molecule of immense versatility with very diverse functions in
482 both the brain and in the periphery (Zelena & Engelmann, 2018). Within the SCN this
483 peptide is important not only as an output signal but also in maintaining synchrony of
484 the SCN network (Shan *et al.*, 2020). A broad view of its potential was suggested
485 decades ago when Gillette and Reppert (Gillette & Reppert, 1987) hypothesized that
486 “Oscillations in AVP secretion and neuronal firing rate potentially represent separate
487 modes by which the SCN transmit time information to other brain regions. The electrical
488 oscillation may relay time-of-day by efferent neuronal output along a limited number of
489 specialized circuits. The AVP secretory rhythm potentially modulates daily rhythm in
490 physiology by a generalized neurohormonal effect.” The present work directs attention
491 to the latter possibility.

492

493 **Figure Legends**

494 **Figure 1.** Lateral ventricle injection sites. Light microscope images of a 50 μ m section
495 showing the injection site for CT β in the lateral ventricle. Some CT β tracer “en passage”
496 is seen in corpus callosum and cortex, but the SCN does not project to these areas.
497 Injection site in (A) is for the SCN shown in Fig. 9, and in (B) for Fig. 10.

498

499 **Figure 2.** Photomicrographs of sagittal sections at mid (left) and lateral (right) SCN from
500 3 representative mice (the most medial aspect of the SCN is not shown). The results
501 indicate that in mid- and lateral-SCN, PER2 positive neurons extend well beyond the
502 borders of AVP neurons. The mice were euthanized at ZT14 (top two panels) and ZT12
503 (bottom panel).

504

505 **Figure 3.** Rostral-caudal differences in AVP neurons. **A.** Confocal images of
506 representative rostral and caudal cells. **B top panel.** Perimeter ($\bar{X} \pm SE$) of rostral vs.
507 caudal cells in all SCN's. **B bottom panel.** Perimeter ($\bar{X} \pm SE$) of neurons within
508 individual SCNs. The lines connect data for rostral and caudal averages within each
509 SCN. **C. top panel.** Volume ($\bar{X} \pm SE$) of rostral vs. caudal cells in all SCNs. **C. bottom**
510 **panel.** Mean volume ($\bar{X} \pm SE$) of neurons within individual SCNs. The lines connect data
511 of average volume for rostral and caudal neurons within each SCN. In all panels, for the
512 estimation statistics, the gray curve indicates the entire range of expected sampling
513 error in measuring the mean. The horizontal blue and magenta lines are the means for
514 the caudal and rostral cells respectively. For all measures, the mean for rostral cells lies
515 far outside the curve indicating a significant difference in size compared to the caudal
516 populations.

517

518 **Figure 4.** Photomicrographs show the relationship of AVP neurons to the CSF in serial
519 sagittal sections from medial to lateral (**A**), and in horizontal sections (**B**). Abbreviations:
520 3V, 3rd ventricle; OCH, optic chiasm.

521

522 **Figure 5.** Photomicrographs of coronal (A,B) and sagittal (C,D) sections through the
523 SCN show extensive AVP projections coursing toward the CSF. A,B,C are light
524 microscopic images of 50 μ m sections and D is a confocal image (z axis: 2 μ m) **A.** Image
525 of a coronal section of the SCN, stained for AVP showing fibers lying close to CSF. The
526 black box delineates the location of the image in B shown at a higher magnification. The
527 black line points to the approximate location of a sagittal section shown in D. **B.** Higher

528 magnification of the same SCN shown in A. Arrows point to AVP fibers projecting to the
529 3rd ventricle. **C.** Sagittal section through mid SCN shows AVP-ir fibers projecting
530 rostrally toward the 3rd ventricle (black arrow). **D.** Confocal image of a sagittal section at
531 the level of the medial SCN [lies at location shown in Fig. 4 (animal #1, image 2)]. Many
532 fibers can be seen coursing towards and possibly crossing the ventricular wall from the
533 SCN to the CSF (z-axis= 2 μ m). 3V: 3rd ventricle; OCH: optic chiasm.

534

535 **Figure 6. A.** Peptidergic content of a biocytin-filled AVP neuron. The montage is
536 created by aligning 1 μ m z-axis confocal images over a z axis of 18 μ m as the process
537 courses through the tissue. The bottom row shows the individual peptides within the
538 biocytin-filled cell. **B.** 3D image of the same cell highlighting the distinct morphological
539 features of axons and dendrites. The axon is thin and beady and the dendrites are
540 thicker and bear varicosities and spines.

541

542 **Figure 7.** Confocal images of sagittal (**A, B, C**) and coronal (**D**) sections stained for
543 AVP (green) and S100 β (magenta), a marker of the ependymal wall. Axons at the level
544 of the SCN cross the ventricular wall into the 3rd ventricle. Boxes in **A, B, C, D** show the
545 areas enlarged in **A', B', C'** and **D'**. **A.** Section of the medial SCN (level 2 in Fig. 4)
546 showing many fibers crossing the ventricular wall (z axis: 2.6 μ m). **A'.** Image showing
547 the 2 branches of an axon reaching the CSF, caudal to the SCN (arrows; z axis: 1 μ m).
548 **B** and **C.** Sections (at level 2 in Fig. 4) show AVP fibers extending dorsally from the
549 SCN, crossing the ependymal wall (z axis: B: 2.6 μ m, C: 3.5 μ m). **B'** and **C'.** Images
550 showing axons crossing the ependymal wall with terminal boutons ending in the 3rd

551 ventricle (arrows; z axis, B' and C': 1.6 μm). **D**. Section showing the SCN and the 3rd
552 ventricle (z axis: 1 μm). D' High magnification images of the area dorsal to the SCN
553 showing an AVP axon coursing on the ventricular side of the ependymal wall (z axis: 0.5
554 μm). SCN: suprachiasmatic nucleus; 3V: 3rd ventricle.

555

556 **Figure 8.** Confocal images of sagittal (**A, B, C**) and coronal (**D**) sections stained for
557 AVP (green) and S100 β (red), a marker of the ependymal wall showing dendrites at the
558 level of the SCN and nearby, crossing the ventricular wall into the 3rd ventricle. Boxes
559 in **A, B, C, D** show the areas enlarged in **A', B', C'** and **D'**. **A**. Section of a mid SCN
560 (image 2 in Fig. 4) showing fibers crossing the ventricular wall (z axis: 7 μm). **A'**. Image
561 showing a large AVP dendrite terminating in the CSF by a bulbous swelling (arrow; z
562 axis: 4 μm). **B**. AVP dendrites extending toward the 3rd ventricle (z axis: 50 μm). **B'**.
563 Image showing a dendrite terminating in the 3rd ventricle by a large terminal bulb
564 (arrow; z axis: 0.25 μm). **C**. Sagittal section of a medial SCN (image 1 on Fig. 4)
565 showing fibers extending toward the 3rd ventricle (z axis: 16 μm). **C'**. Image showing
566 two dendrites terminating in the 3rd ventricle (arrows, z axis: 2.5 μm). **D**. Coronal
567 section showing the SCN and the 3rd ventricle (z axis: 4.3 μm). **D'**. Image showing a
568 large dendrite, dorsal to the SCN, crossing the ventricular wall, ending in the 3rd
569 ventricle (arrow, z axis: 2.5 μm). SCN: suprachiasmatic nucleus; 3V: 3rd ventricle.

570

571 **Figure 9:** Confocal images (z axis: 4 μm) of an SCN stained for CT β (magenta), AVP
572 (green) and double-labelled. Inset is an image of a cell double labelled for CT β +AVP (z
573 axis: 1 micron).

574

575 **Figure 10.** The photomicrographs show the full extent of the SCN in sagittal view from
576 its medial to lateral-most aspect in sections labelled for CT β (magenta, left column), and
577 CT β +AVP (right column). The SCN, outlined in white dots, indicates the area used to
578 count cells.

579

580 **References**

- 581 ABRAHAMSON, E. E. & MOORE, R. Y. 2001. Suprachiasmatic nucleus in the mouse: retinal
582 innervation, intrinsic organization and efferent projections. *Brain Res*, 916, 172-91.
- 583 ANTLE, M. C. & SILVER, R. 2005. Orchestrating time: arrangements of the brain circadian
584 clock. *Trends Neurosci*, 28, 145-51.
- 585 BERK, M. L. & FINKELSTEIN, J. A. 1981. An autoradiographic determination of the efferent
586 projections of the suprachiasmatic nucleus of the hypothalamus. *Brain Res*, 226, 1-13.
- 587 BROWN, M. H. & NUNEZ, A. A. 1989. Vasopressin-deficient rats show a reduced amplitude of
588 the circadian sleep rhythm. *Physiol Behav*, 46, 759-62.
- 589 BRUNNER, J., KECK, M. E., LANDGRAF, R., UHR, M., NAMENDORF, C. & BRONISCH, T.
590 2002. Vasopressin in CSF and plasma in depressed suicide attempters: preliminary
591 results. *Eur Neuropsychopharmacol*, 12, 489-94.
- 592 CAMPOS, L. M., CRUZ-RIZZOLO, R. J., WATANABE, I. S., PINATO, L. & NOGUEIRA, M. I.
593 2014. Efferent projections of the suprachiasmatic nucleus based on the distribution of
594 vasoactive intestinal peptide (VIP) and arginine vasopressin (AVP) immunoreactive
595 fibers in the hypothalamus of *Sapajus apella*. *J Chem Neuroanat*, 57-58, 42-53.

- 596 CARD, J. P. & MOORE, R. Y. 1984. The suprachiasmatic nucleus of the golden hamster:
597 immunohistochemical analysis of cell and fiber distribution. *Neuroscience*, 13, 415-431.
- 598 CARLEN, M., MELETIS, K., GORITZ, C., DARSALIA, V., EVERGREN, E., TANIGAKI, K.,
599 AMENDOLA, M., BARNABE-HEIDER, F., YEUNG, M. S., NALDINI, L., HONJO, T.,
600 KOKAIA, Z., SHUPLIAKOV, O., CASSIDY, R. M., LINDVALL, O. & FRISEN, J. 2009.
601 Forebrain ependymal cells are Notch-dependent and generate neuroblasts and
602 astrocytes after stroke. *Nat Neurosci*, 12, 259-67.
- 603 CASSONE, V. M., SPEH, J. C., CARD, J. P. & MOORE, R. Y. 1988. Comparative anatomy of
604 the mammalian hypothalamic suprachiasmatic nucleus. *J. Biol. Rhythms*, 3, 71-91.
- 605 COCCARO, E. F., KAVOUSSI, R. J., HAUGER, R. L., COOPER, T. B. & FERRIS, C. F. 1998.
606 Cerebrospinal fluid vasopressin levels: correlates with aggression and serotonin function
607 in personality-disordered subjects. *Arch Gen Psychiatry*, 55, 708-14.
- 608 DAI, J., SWAAB, D. F. & BUIJS, R. M. 1997. Distribution of vasopressin and vasoactive
609 intestinal polypeptide (VIP) fibers in the human hypothalamus with special emphasis on
610 suprachiasmatic nucleus efferent projections. *J Comp Neurol*, 383, 397-414.
- 611 DAIKOKU, S., HISANO, S. & KAGOTANI, Y. 1992. Neuronal associations in the rat
612 suprachiasmatic nucleus demonstrated by immunoelectron microscopy. *J. Comp.*
613 *Neurol.*, 325, 559-571.
- 614 DE VRIES, G. J. & MILLER, M. A. 1998. Anatomy and function of extrahypothalamic
615 vasopressin systems in the brain. *Prog Brain Res*, 119, 3-20.
- 616 DIDIER, M., HARANDI, M., AGUERA, M., BANCEL, B., TARDY, M., FAGES, C., CALAS, A.,
617 STAGAARD, M., MOLLGARD, K. & BELIN, M. F. 1986. Differential immunocytochemical
618 staining for glial fibrillary acidic (GFA) protein, S-100 protein and glutamine synthetase in

- 619 the rat subcommissural organ, nonspecialized ventricular ependyma and adjacent
620 neuropil. *Cell Tissue Res*, 245, 343-51.
- 621 DROUYER, E., LESAUTER, J., HERNANDEZ, A. L. & SILVER, R. 2010. Specializations of
622 gastrin-releasing peptide cells of the mouse suprachiasmatic nucleus. *J Comp Neurol*,
623 518, 1249-63.
- 624 GILLETTE, M. U. & REPERT, S. M. 1987. The hypothalamic suprachiasmatic nuclei: circadian
625 patterns of vasopressin secretion and neuronal activity *in vitro*. *Brain Res. Bull.*, 19, 135-
626 139.
- 627 GROBLEWSKI, T. A., NUNEZ, A. A. & GOLD, R. M. 1981. Circadian rhythms in vasopressin
628 deficient rats. *Brain Res. Bull.*, 6, 125-130.
- 629 HO, L. H., RUFFIN, R. E., MURGIA, C., LI, L., KRILIS, S. A., & ZALEWSKI, P. D. 2004. Labile zinc
630 and zinc transporter ZnT4 in mast cell granules: Role in regulation of caspase activation and
631 NF- κ B translocation. *J. Immunol.*, **172**, 7750– 7760.
- 632 HONMA, S. 2020. Development of the circadian clock. *Eur. J. Neurosci.*, 51, 182-193.
- 633 HOORNEMAN, E. M. D. & BUIJS, R. M. 1982. Vasopressin fiber pathways in the rat brain
634 following suprachiasmatic nucleus lesioning. *Brain Res.*, 243, 235-241.
- 635 JIN, X., SHEARMAN, L. P., WEAVER, D. R., ZYLKA, M. J., DE VRIES, G. J. & REPERT, S.
636 M. 1999. A molecular mechanism regulating rhythmic output from the suprachiasmatic
637 nucleus. *Cell*, 96, 57-68.
- 638 JOLKKONEN, J., TUOMISTO, L., VAN WIMERSMA GREIDANUS, T. B. & RIEKKINEN, P. J.
639 1988. Vasopressin levels in the cerebrospinal fluid of rats with lesions of the
640 paraventricular and suprachiasmatic nuclei. *Neurosci. Lett.*, 86, 184-188.

- 641 KAGERBAUER, S. M., MARTIN, J., SCHUSTER, T., BLOBNER, M., KOCHS, E. F. &
642 LANDGRAF, R. 2013. Plasma oxytocin and vasopressin do not predict neuropeptide
643 concentrations in human cerebrospinal fluid. *J Neuroendocrinol*, 25, 668-73.
- 644 KALSBECK, A., FLIERS, E., HOFMAN, M. A., SWAAB, D. F. & BUIJS, R. M. 2010. Vasopressin
645 and the output of the hypothalamic biological clock. *J Neuroendocrinol*, 22, 362-72.
- 646 KALSBECK, A., TECLEMARIAM-MESBAH, R. & PÉVET, P. 1993. Efferent projections of the
647 suprachiasmatic nucleus in the golden hamster (*mesocricetus auratus*). *J. Comp.*
648 *Neurol.*, 332, 293-314.
- 649 KUHLMAN, S. J., QUINTERO, J. E. & MCMAHON, D. G. 2000. GFP fluorescence reports
650 Period1 circadian gene regulation in the mammalian biological clock. *NeuroReport*, 11,
651 1479-1482.
- 652 LAVADO, A. & OLIVER, G. 2011. Six3 is required for ependymal cell maturation. *Development*,
653 138, 5291-300.
- 654 LEAK, R. K. & MOORE, R. Y. 2001. Topographic organization of suprachiasmatic nucleus
655 projection neurons. *J Comp Neurol*, 433, 312-34.
- 656 LEAK, R. K. & MOORE, R. Y. 2012. Innervation of ventricular and periventricular brain
657 compartments. *Brain Res*, 1463, 51-62.
- 658 LEE, M. L., SWANSON, B. E. & DE LA IGLESIA, H. O. 2009. Circadian timing of REM sleep is
659 coupled to an oscillator within the dorsomedial suprachiasmatic nucleus. *Curr Biol*, 19,
660 848-52.
- 661 LESAUTER, J. & SILVER, R. 1998. Output signals of the SCN. *Chronobiol Int*, 15, 535-50.
- 662 LOKSHIN, M., LESAUTER, J. & SILVER, R. 2015. Selective Distribution of Retinal Input to
663 Mouse SCN Revealed in Analysis of Sagittal Sections. *J Biol Rhythms*, 30, 251-7.

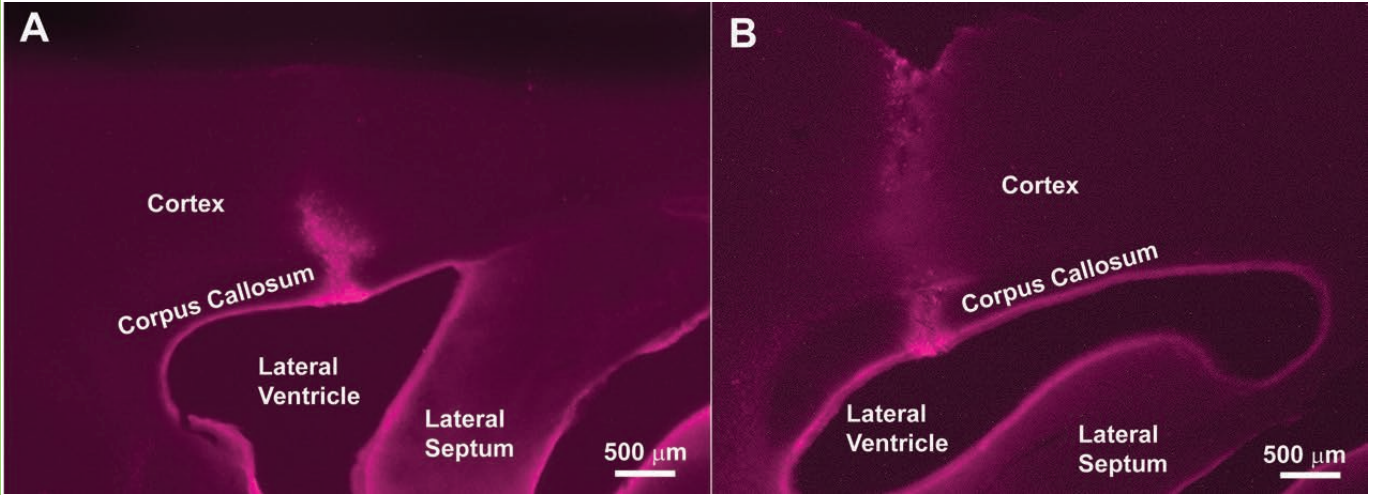
- 664 MASUMOTO, K. H., NAGANO, M., TAKASHIMA, N., HAYASAKA, N., HIYAMA, H.,
665 MATSUMOTO, S., INOUE, S. T. & SHIGEYOSHI, Y. 2006. Distinct localization of
666 prokineticin 2 and prokineticin receptor 2 mRNAs in the rat suprachiasmatic nucleus. *Eur*
667 *J Neurosci*, 23, 2959-70.
- 668 MAYWOOD, E. S., CHESHAM, J. E., O'BRIEN, J. A. & HASTINGS, M. H. 2011. A diversity of
669 paracrine signals sustains molecular circadian cycling in suprachiasmatic nucleus
670 circuits. *Proc Natl Acad Sci U S A*, 108, 14306-11.
- 671
- 672 MIEDA, M., ONO, D., HASEGAWA, E., OKAMOTO, H., HONMA, K., HONMA, S. & SAKURAI,
673 T. 2015. Cellular clocks in AVP neurons of the SCN are critical for interneuronal coupling
674 regulating circadian behavior rhythm. *Neuron*, 85, 1103-16.
- 675 MOORE, R. Y. 2013. The suprachiasmatic nucleus and the circadian timing system. *Prog Mol*
676 *Biol Transl Sci*, 119, 1-28.
- 677 MOORE, R. Y. & SILVER, R. 1998. Suprachiasmatic nucleus organization. *Chronobiol Int*, 15,
678 475-87.
- 679 MOORE, R. Y., SPEH, J. C. & LEAK, R. K. 2002. Suprachiasmatic nucleus organization. *Cell*
680 *Tissue Res*, 309, 89-98.
- 681 MORIN, L. P. 1994. The circadian visual system. *Brain Res. Rev.*, 67, 102-127.
- 682 MORIN, L. P. 2013. Neuroanatomy of the extended circadian rhythm system. *Exp Neurol*, 243,
683 4-20.
- 684 MORIN, L. P. & ALLEN, C. N. 2006. The circadian visual system, 2005. *Brain Res Brain Res*
685 *Rev.*
- 686

- 687 OZTAN, O., GARNER, J. P., PARTAP, S., SHERR, E. H., HARDAN, A. Y., FARMER, C.,
688 THURM, A., SWEDO, S. E. & PARKER, K. J. 2018. Cerebrospinal fluid vasopressin and
689 symptom severity in children with autism. *Ann Neurol*, 84, 611-615.
- 690 RAMANATHAN, C., NUNEZ, A. A., MARTINEZ, G. S., SCHWARTZ, M. D. & SMALE, L. 2006.
691 Temporal and spatial distribution of immunoreactive PER1 and PER2 proteins in the
692 suprachiasmatic nucleus and peri-suprachiasmatic region of the diurnal grass rat
693 (*Arvicanthis niloticus*). *Brain Res*, 1073-1074, 348-58.
- 694 RIDDLE, M., MEZIAS, E., FOLEY, D., LESAUTER, J. & SILVER, R. 2017. Differential
695 localization of PER1 and PER2 in the brain master circadian clock. *Eur J Neurosci*, 45,
696 1357-1367.
- 697 SCHWARTZ, W. J., COLEMAN, R. J. & REPERT, S. M. 1983. A daily vasopressin rhythm in
698 rat cerebrospinal fluid. *Brain Res.*, 263, 105-112.
- 699 SCHWARTZ, W. J. & REPERT, S. M. 1985. Neural regulation of the circadian vasopressin
700 rhythm in cerebrospinal fluid: a pre-eminent role for the suprachiasmatic nuclei. *J.*
701 *Neurosci.*, 5, 2771-2778.
- 702 SHAN, Y., ABEL, J. H., LI, Y., IZUMO, M., COX, K. H., JEONG, B., YOO, S. H., OLSON, D. P.,
703 DOYLE, F. J., 3RD & TAKAHASHI, J. S. 2020. Dual-Color Single-Cell Imaging of the
704 Suprachiasmatic Nucleus Reveals a Circadian Role in Network Synchrony. *Neuron*.
- 705 SILVER, R., LESAUTER, J., TRESKO, P. A. & LEHMAN, M. N. 1996. A diffusible coupling
706 signal from the transplanted suprachiasmatic nucleus controlling circadian locomotor
707 rhythms. *Nature*, 382, 810-813.
- 708 SILVER, R., SOOKHOO, A. I., LESAUTER, J., STEVENS, P., JANSEN, H. T. & LEHMAN, M.
709 N. 1999. Multiple regulatory elements result in regional specificity in circadian rhythms of
710 neuropeptide expression in mouse SCN. *NeuroReport*, 10, 3165-3174.

- 711 SÖDERSTEIN, P., DEVRIES, G. J., BUIJS, R. M. & MELIN, P. 1985. A daily rhythm in
712 behavioral vasopressin sensitivity and brain vasopressin concentrations. *Neurosci. Lett.*,
713 58, 37-41.
- 714 SOFRONIEW, M. V. & WEINDL, A. 1980. Identification of parvocellular vasopressin and
715 neurophysin neurons of the suprachiasmatic nucleus of a variety of mammals including
716 primates. *J. Comp. Neurol.*, 193, 659-675.
- 717 STARK, R. I. & DANIEL, S. S. 1989. Circadian rhythm of vasopressin levels in cerebrospinal
718 fluid of the fetus: effect of continuous light. *Endocrinology*, 124, 3095-101.
- 719 STEPHAN, F. K., BERKLEY, K. J. & MOSS, R. L. 1981. Efferent connections of the rat
720 suprachiasmatic nucleus. *Neuroscience*, 6, 2625-2641.
- 721 SWAAB, D. F., BAO, A. M. & LUCASSEN, P. J. 2005. The stress system in the human brain in
722 depression and neurodegeneration. *Ageing Res Rev*, 4, 141-94.
- 723 TECLEMARIAM-MESBAH, R., TER HORST, G. J., POSTEMA, F., WORTEL, J. & BUIJS, R. M.
724 1999. Anatomical demonstration of the suprachiasmatic nucleus-pineal pathway. *J*
725 *Comp Neurol*, 406, 171-82.
- 726 TOKUDA, I. T., ONO, D., HONMA, S., HONMA, K. I. & HERZEL, H. 2018. Coherency of
727 circadian rhythms in the SCN is governed by the interplay of two coupling factors. *PLoS*
728 *Comput Biol*, 14, e1006607.
- 729 UHEYAMA, T., KROUT, K. E., NGUYEN, X. V., KARPITSKIY, V., KOLLERT, A.,
730 METTENLEITER, T. C. & LOEWY, A. D. 1999. Suprachiasmatic nucleus: a central
731 autonomic clock. *Nat Neurosci*, 2, 1051-3.
- 732 VAN DEN POL, A. N. 1980. The hypothalamic suprachiasmatic nucleus of rat: intrinsic
733 anatomy. *J. Comp. Neurol.*, 191, 661-702.
- 734 VAN DEN POL, A. N. 2012. Neuropeptide transmission in brain circuits. *Neuron*, 76, 98-115.

- 735 VAN DEN POL, A. N. & TSUJIMOTO, K. L. 1985. Neurotransmitters of the hypothalamic
736 suprachiasmatic nucleus: immunocytochemical analysis of 25 neuronal antigens.
737 *Neuroscience*, 15, 1049-86.
- 738 VANDESANDE, F., DIERICKX, K. & DEMEY, J. 1975. Identification of the vasopressin-
739 neurophysin producing neurons of the rat suprachiasmatic nuclei. *Cell Tissue Res*, 156,
740 377-80.
- 741 VARADARAJAN, S., TAJIRI, M., JAIN, R., HOLT, R., AHMED, Q., LESAUTER, J. & SILVER, R.
742 2018. Connectome of the Suprachiasmatic Nucleus: New Evidence of the Core-Shell
743 Relationship. *eNeuro*, 5.
- 744 WATTS, A. G. & SWANSON, L. W. 1987. Efferent projections of the suprachiasmatic nucleus:
745 II. Studies using retrograde transport of fluorescent dyes and simultaneous peptide
746 immunohistochemistry in the rat. *J. Comp. Neurol.*, 258, 230-252.
- 747 WATTS, A. G., SWANSON, L. W. & SANCHEZ-WATTS, G. 1987. Efferent projections of the
748 suprachiasmatic nucleus: I. Studies using anterograde transport of *Phaseolus vulgaris*
749 leucoagglutinin in the rat. *J. Comp. Neurol.*, 258, 204-229.
- 750 WELSH, D. K., TAKAHASHI, J. S. & KAY, S. A. 2010. Suprachiasmatic nucleus: cell autonomy
751 and network properties. *Annu Rev Physiol*, 72, 551-77.
- 752 WILLIAMS, W. P., 3RD, JARJISIAN, S. G., MIKKELSEN, J. D. & KRIEGSFELD, L. J. 2011.
753 Circadian control of kisspeptin and a gated GnRH response mediate the preovulatory
754 luteinizing hormone surge. *Endocrinology*, 152, 595-606.
- 755 XIAO, M., DING, J., WU, L., HAN, Q., WANG, H., ZUO, G. & HU, G. 2005. The distribution of
756 neural nitric oxide synthase-positive cerebrospinal fluid-contacting neurons in the third
757 ventricular wall of male rats and coexistence with vasopressin or oxytocin. *Brain Res*,
758 1038, 150-62.

759 ZELENA, D. & ENGELMANN, M. 2018. The Brattleboro Rat: The First and Still Up-to-Date
760 Mutant Rodent Model for Neuroendocrine Research *In*: LUDWIG, M. & LEVKOWITZ, G.
761 (eds.) *Model animals in neuroendocrinology : from worm to mouse to man*. First edition.
762 ed. Hoboken, NJ: Wiley.
763



Mid-SCN

Lateral SCN

AVP-PER2

Rostral

Caudal

100 μ m

